



Ahmadi, E., Alexander, N. A., & Kashani, M. (2019). Lateral dynamic bridge deck-pier interaction for ultra-high-speed Hyperloop train loading. *Proceedings of the ICE - Bridge Engineering*.  
<https://doi.org/10.1680/jbren.19.00011>

Peer reviewed version

Link to published version (if available):  
[10.1680/jbren.19.00011](https://doi.org/10.1680/jbren.19.00011)

[Link to publication record in Explore Bristol Research](#)  
PDF-document

This is the author accepted manuscript (AAM). The final published version (version of record) is available online via Thomas Telford (ICE Publishing) at <https://www.icevirtuallibrary.com/doi/abs/10.1680/jbren.19.00011> . Please refer to any applicable terms of use of the publisher.

## University of Bristol - Explore Bristol Research

### General rights

This document is made available in accordance with publisher policies. Please cite only the published version using the reference above. Full terms of use are available:  
<http://www.bristol.ac.uk/red/research-policy/pure/user-guides/ebr-terms/>

# Accepted manuscript doi: 10.1680/jbren.19.00011

---

## **Accepted manuscript**

As a service to our authors and readers, we are putting peer-reviewed accepted manuscripts (AM) online, in the Ahead of Print section of each journal web page, shortly after acceptance.

## **Disclaimer**

The AM is yet to be copyedited and formatted in journal house style but can still be read and referenced by quoting its unique reference number, the digital object identifier (DOI). Once the AM has been typeset, an 'uncorrected proof' PDF will replace the 'accepted manuscript' PDF. These formatted articles may still be corrected by the authors. During the Production process, errors may be discovered which could affect the content, and all legal disclaimers that apply to the journal relate to these versions also.

## **Version of record**

The final edited article will be published in PDF and HTML and will contain all author corrections and is considered the version of record. Authors wishing to reference an article published Ahead of Print should quote its DOI. When an issue becomes available, queuing Ahead of Print articles will move to that issue's Table of Contents. When the article is published in a journal issue, the full reference should be cited in addition to the DOI.

**Submitted:** 20 March 2019

**Published online in ‘accepted manuscript’ format:** 20 September 2019

**Manuscript title:** Lateral dynamic bridge deck-pier interaction for ultra-high-speed  
Hyperloop train loading

**Authors:** Ehsan Ahmadi<sup>1</sup>, Nicholas A. Alexander<sup>2</sup> and Mohammad M. Kashani<sup>1</sup>

**Affiliations:** <sup>1</sup>Faculty of Engineering and Physical Sciences, University of Southampton, UK  
and <sup>2</sup>Department of Civil Engineering, University of Bristol, UK

**Corresponding author:** Ehsan Ahmadi, Faculty of Engineering and Physical Sciences,  
University of Southampton, UK.

**E-mail:** e.ahmadi@soton.ac.uk

## **Abstract**

The next generation of ultra-high-speed (UHS) trains, known as Hyperloop and TransPod, are aerospace type vehicles designed to carry passengers. The UHS employs a vehicle capsule within a protected vacuum tube deck, supported by reinforced concrete piers (i.e. multi-span viaduct). The tube environment allows multiple UHS vehicles to run in parallel simultaneously (i.e. twin tube deck) where asymmetric train loading will result in a large dynamic unbalanced moment on the piers. Therefore, exploring the lateral dynamic interaction of bridge deck (twin tube) and piers under such an unbalanced moment is an extremely important factor for analysis of viaducts under dynamic UHS train loading. Hence, this paper analytically addresses the dynamic bridge deck-pier interaction under UHS train loading for lateral vibration.

**Keywords:** bridges; railway systems; dynamics; lateral bridge deck-pier interaction; ultra-high-speed Hyperloop train; dynamic amplification factor

## 1. Introduction

Hyperloops, first proposed by Tesla, and later by TransPod, are passenger and freight transportation modes at ultra-high speeds (UHS), and are composed of a number of vacuum tubes (Janzen 2017). Within these tubes, pods can move free of air resistance or friction transporting passengers and cargo. Furthermore, Hyperloops use magnetic levitation and linear accelerators to push the pods forward. The operating speed of these UHS trains is around 970 km/h up to a maximum speed of 1200 km/h, and is far higher compared to 270 km/h for mean operating speed of high-speed (HS) trains. The current UK network rail document (Network Rail, 2006) for structural design and assessment of bridges ignores vertical dynamic effects of moving loads for train speeds below 160 km/h e.g. vertical dynamic amplification factor (DAF) of 1. Nonlinear analysis of existing UK railway bridges also suggests that dynamic train loading plays a key role for train speeds higher than 160 km/h ((Parke & Hewson 2008),(Canning & Kashani 2016)). Eurocode EN 1991-2 (2003) uses similar approach for calculation of vertical DAFs for train speeds not more than 200 km/h. However, for train speeds over 200 km/h, Eurocode EN 1991-2 (2003) recommends further rigorous dynamic analysis for calculation of vertical DAFs.

The UHS train usually moves at speed of around four times the mean speed of conventional HS trains. At these ultra-high speeds, dynamic amplification might be very high, and DAFs for UHS trains are of great importance for safe design purposes. In addition, Hyperloop tubes will be supported by multiple piers, which vertically support the tubes and longitudinally allow for the displacement of the tubes due to the thermal expansion. For example in the proposed San Francisco-Los Angeles route, the mean spacing of the piers is 30m and around 25000 piers are required for the entire line (Musk 2013). Alexander and Kashani (2018) analytically investigated DAFs due to UHS Hyperloop trains for vertical motion through a parametric analysis. They found that the UHS Hyperloop trains can introduce very large

vertical DAFs and as such, the current design recommendations are inadequate for the design of these systems. However, the Hyperloop tube-bridge pier interaction is yet to be investigated for lateral motion of the deck. In this study, the lateral vibration of the deck comes from asymmetric train loading where not all but some tubes are loaded. However, lateral loadings such as earthquake and to a lesser extent, wind, can cause lateral vibrations which do not fall within the scope of this study.

The moving load problem was first mathematically described by Timoshenko (Timoshenko 1922) and in a comprehensive and detailed report by Frýba (1972) that explains formulation of moving force and moving mass for simple spans. Moving force-beam systems were also formulated to address vertical vehicle-bridge interaction problems ((Filho 1978),(Olsson 1985),(Olsson 1991),(Wu et al. 2000)). Similarly, a comprehensive work on the formulation of human-structure systems was carried out by Caprani and Ahmadi (2016) for use in vertical human-induced vibrations. Analytical solutions to moving load problems are beneficial for parametric analyses. However, all moving force problems cannot be analytically solved and more detailed numerical methods are required to determine vibration response of such systems (Olsson 1991). Moving load problems can be treated as static loads applying to different positions on a structure for simplicity. However, dynamic effects of moving loads can be pronounced in particular for HS trains. Thus, DAFs are defined as dynamic-to-quasi static peak deflection or stress caused by the dynamics of moving loads. A solid literature review on DAFs of road bridges for vertical motion can be found in (Paultre et al. 1992). There is currently limited analytical and numerical study available in the literature on UHS Hyperloop trains, and hence, there is no design guideline to help bridge engineers to design bridges to accommodate the next-generation UHS transport system. As previously stated, although DAFs of UHS Hyperloop trains have been already addressed for vertical vibration,

the DAFs of such systems need be investigated for lateral vibration due to the eccentricity of train loadings. Hence, this paper is the first attempt to numerically investigate lateral vibration of Hyperloop train-bridge-pier systems. Therefore, this study analytically investigates lateral DAFs of Hyperloop train-bridge-pier systems through a parametric analysis. To achieve this goal, Hyperloop train is modelled as a series of moving masses and energy equation of the system is written to derive equation of motion for lateral direction. The dynamic of the system is then described in terms of non-dimensional parameters for lateral vibration, and lateral DAFs are determined and discussed.

## 2. Modelling Approach

In this section, the equation of lateral motion of a bridge deck-pier system under asymmetrical train loading is derived. As shown in Figure 1, the bridge deck is considered as two parallel continuous Hyperloop tube beams of span length  $L$  and number of spans  $n_s$ . The train is modelled as a series of equal moving masses,  $m_p$ , with constant velocity,  $v$ , travelling across one of the Hyperloop tube beams, i.e. asymmetrical dynamic loading. Hyperloop is not a typical train in the conventional sense, it is like a ‘bullet’, travelling at great speeds through a near vacuum tube. As the train levitates, the gravitational forces (on the train) must be transmitted through magnetic fields to the tube. For the train to respond to centrifugal effects on curved sections of track and to accommodate lateral motions of the deck, the magnetic forces must have both lateral and vertical components. It should be also noted that the exact form of an equivalent sprung-damped moving mass system for the hyperloop trains has not been defined yet as physical prototypes are still an ongoing design problem. Hence, we conclude that a moving mass formulation includes both a moving gravitational force where the system changes in mass with time is a more general problem specification. The mass per unit length and lateral flexural rigidity of both beams together are  $m_b$  and  $EI_b$  and lateral flexural rigidity of each column (bridge pier) of height  $h$  is  $EI_c$ . Small deflection theory and

linear elastic analysis are used to formulate the lateral motion of the deck. Torsional and vertical oscillations are also ignored in this analysis.

## 2.1 Energy terms of the system in physical space

The kinetic energy of the system,  $Q$ , emanates from two terms: (1) the kinetic energy of the beams, and (2) the kinetic energy of the moving trainset:

$$Q = \frac{1}{2} m_b \int_0^{n_s L} \dot{y}^2 dx + \frac{1}{2} \sum_{p=1}^{n_p} \left\{ \beta(x_p) m_p \dot{y}(x_p, t)^2 \right\} \quad (1)$$

where  $y(x, t)$  is the lateral spatiotemporal displacement of the Hyperloop tubes, and  $m_p$  is the mass of the  $p$ th load in the trainset of  $n_p$  moving point loads. The boxcar function  $\beta(x)$  ensures that only the travelling masses “on the beams” are considered in this energy calculation. The boxcar function is defined as follows

$$\beta(x) = H(x) - H(x - n_s L) \quad (2)$$

where  $H(x)$  is the Heaviside function. A non-dimensional coordinate  $\xi$  is introduced where  $x = \xi L$ , and the train positions  $x_p = \xi_p L$ . Hence, equation (1) can be restated as

$$Q = \frac{m_b L}{2} \int_0^{n_s} \dot{y}^2 d\xi + \frac{1}{2} \sum_{p=1}^{n_p} \left\{ \beta(\xi_p) m_p \dot{y}(\xi_p, t)^2 \right\} \quad (3)$$

Note that this change of variable changes the integral limits in the standard way. The potential energy,  $V$ , of the system comes from three terms: (1) the lateral flexural energy in deforming the Hyperloop beam tubes, (2) the flexural energy in laterally deforming the cantilever columns when subjected to an end moment, and (3) the external work done again laterally by the gravitational induced moment (large deformation P- $\Delta$  effects are ignored)

$$V = \frac{1}{2} \int_0^{n_s L} EI_b y''^2 dx + \frac{1}{2} \sum_{k=0}^{n_s} \left\{ \frac{4EI_c}{h^3} y(x_k, t)^2 \right\} - \sum_{p=1}^{n_p} \left\{ \beta(x_p) \int f_p e d\theta_p(x_p) \right\} \quad (4)$$

where the  $p$ th vertical gravity load is  $f_p = m_p g$ , the eccentricity of this vertical load is  $e$  which is half the horizontal spacing of the tubes and  $\theta_p$  is the rotation at the top of the cantilever



columns. From structural mechanics, the relationship between top rotation,  $\theta_p$ , and top displacement,  $y$ , of the columns is given by  $\theta_p = -2y/h$ . This assumption is reasonably valid for bridges longer than 40m. Hence, this relationship is used as an approximation for the relationship between beams rotation and lateral displacement. In this way, we can completely remove rotational degrees of freedom (DOFs) and consider only lateral translational DOFs.

Hence, equation (4) becomes:

$$V = \frac{EI_b}{2L^3} \int_0^{n_s} y''^2 d\xi + \frac{1}{2} \sum_{k=0}^{n_s} \left\{ \frac{4EI_c}{h^3} y(\xi_k, t)^2 \right\} + \sum_{p=1}^{n_p} \left\{ \beta(\xi_p) \frac{2m_p g e}{h} \int dy_p(\xi_p) \right\} \quad (5)$$

## 2.2 Equation of motion in modal space

To employ the minimisation of action principle (Euler-Lagrange equations of motion), a spatiotemporal expansion of the beam displacement is introduced:

$$y(\xi, t) = \sum_{i=1}^q \left\{ \phi_i(\xi) u_i(t) \right\} = \begin{bmatrix} \phi_1, \dots, \phi_q \end{bmatrix} \begin{bmatrix} u_1 \\ \vdots \\ u_q \end{bmatrix} = \boldsymbol{\phi}^T \mathbf{u} \quad (6)$$

where  $\phi_i$  elements are spatial part of the beams response and  $u_i$  elements are temporal part of the beams response ( $q$  DOFs).  $\phi_i(\xi)$  elements are ideally a good representation of the mode shapes of the system which guarantee a reliable dynamical model of the system with a small number of DOFs  $q$ . However, we may select any set of functions for  $\phi_i(\xi)$  that satisfy the boundary conditions of the beams at the supports (columns' location). Using equations (3), (5), and (6), the tensorial form of the Lagrangian (kinetic minus potential energies) of the system normalised by  $m_b L$  is written as:

$$\frac{\Pi}{m_b L} = \frac{1}{2} (M_{ij}^b + M_{ij}^t) \dot{u}_i \dot{u}_j - \frac{1}{2} (K_{ij}^b + K_{ij}^c) u_i u_j - F_j^t \int du_j \quad (7)$$

in which  $u_i$  elements are approximately modal amplitudes;  $\Pi$  is the Lagrangian, and  $u_j$  is the lateral displacement at the  $j$ th support. The rank 2 tensors (mass matrices) in equation (7) are given by:

$$M_{ij}^b = \int_0^{n_s} \phi_i \phi_j d\xi, \quad M_{ij}^t = \sum_{p=1}^{n_p} \left\{ \beta(\xi_p) \alpha_p \phi_i(\xi_p) \phi_j(\xi_p) \right\} \quad (8)$$

where  $M_{ij}^b$  is the bridge mass matrix and  $M_{ij}^t$  is the travel load (trainset) mass matrix. Similarly, the stiffness matrices are defined as follows,

$$K_{ij}^b = \omega^2 \int_0^{n_s} \phi_i'' \phi_j'' d\xi, \quad K_{ij}^c = \eta \omega^2 \sum_{k=0}^{n_s} \left\{ \phi_i(\xi_k) \phi_j(\xi_k) \right\} \quad (9)$$

where  $K_{ij}^b$  is the bridge (deck beam) stiffness matrix and  $K_{ij}^c$  is the supports (columns) stiffness matrix. Finally, the traveling load vector is defined as:

$$F_j^t = 2g\varepsilon \sum_{p=1}^{n_p} \left\{ \beta(\xi_p) \alpha_p \phi_j(\xi_p) \right\} \quad (10)$$

where  $F_j^t$  is the vector of time-dependant loads due to the travelling trainset. These, matrices and vectors are defined in terms of the following system parameters,

$$\alpha_p = \frac{m_p}{m_b L}, \quad \omega^2 = \frac{EI_b}{m_b L^4}, \quad \eta = \frac{4EI_c}{h^3} \frac{L^3}{EI_b}, \quad \varepsilon = \frac{e}{h} \quad (11)$$

where  $\alpha_p$  is the mass ratio of the  $p$ th trainset mass to the mass (per span) of the two parallel Hyperloop tube beams,  $\omega$  is the frequency parameter,  $\eta$  is the ratio of column to beam flexural stiffness, and  $\varepsilon$  is an eccentricity ratio of the tube. By employing the vectorial form of the Euler-Lagrange equation (equation (7)), the equation of motion is given by:

$$\left( M_{ij}^b + M_{ij}^t \right) \ddot{u}_i + \left( K_{ij}^b + K_{ij}^c \right) u_i = F_j^t \quad (12)$$

To satisfy boundary conditions of the multi-span continuous beams at the supports (lateral displacements), terms of a Fourier series are adopted as an approximation to modal basis for an  $n_s$ -span beam

$$\phi_i(\xi) = \begin{bmatrix} 1 \\ \sin(\pi\xi/n_s) \\ \cos(\pi\xi/n_s) \\ \vdots \\ \sin(k\pi\xi/n_s) \\ \cos(k\pi\xi/n_s) \end{bmatrix} \in \mathbb{R}^{q \times 1} \quad (13)$$

The number of DOFs is given by  $q$  where  $q = 2k + 1$  where  $k \geq n_s$ . This partial Fourier series includes a half-sine wave across the entire bridge length  $n_s L$ , a half-sine wave for an individual span  $L$  and further higher modes if  $k > n_s$ . Hence, both primary modes for flexible and stiff columns are considered.

### 2.3 Equation of motion in a non-dimensional form

To describe equation (12) in a non-dimensional form, approximate modal amplitudes and time are normalised as

$$u = \frac{g}{\omega_{1l}^2} z, \quad t = \frac{\tau}{\omega_{1l}} \quad (14)$$

where  $\tau$  and  $z$  are normalised time and displacement respectively;  $\omega_{1l}$  is the first natural frequency of the unloaded bridge for lateral motion. By substituting equation (14) into equation (12) and adding Rayleigh damping term of the beams,  $C_{ij} \dot{z}_i$ , and rearranging, we obtain:

$$\left( M_{ij}^b + M_{ij}^t \right) \ddot{z}_i + C_{ij} \dot{z}_i + \left( K_{ij}^{b*} + \eta K_{ij}^{c*} \right) z_i = F_j^{t*} \quad (15)$$

Note that a stiffness-proportional damping is used for the beams; the normalised stiffness matrices are defined as follows,

$$K_{ij}^{b*} = \sigma^2 \int_0^{n_s} \phi_i'' \phi_j'' d\xi, \quad K_{ij}^{c*} = \sigma^2 \sum_{k=0}^{n_s} \left\{ \phi_i(\xi_k) \phi_j(\xi_k) \right\}, \quad \sigma = \frac{\omega}{\omega_{1l}} \quad (16)$$

and the damping matrix is define as

$$C_{ij} = a_1 M_{ij}^b + a_2 \left( K_{ij}^{b*} + \eta K_{ij}^{c*} \right) \quad (17)$$

where coefficients  $a_1$  and  $a_2$  are obtained in the standard way from (see (Cruz & Miranda 2017)) using the first and second modes. The normalised loading vectors is as follows,

$$F_j^{t*} = 2\varepsilon \sum_{p=1}^{n_p} \left\{ \beta(\xi_p) \alpha_p \phi_j(\xi_p) \right\} \quad (18)$$

The modal natural frequencies of the beams are determined from eigenvalues of dynamic matrix  $(M_{ij}^b)^{-1}(K_{ij}^{b*} + \eta K_{ij}^{c*})$ . We also assume the same damping ratio,  $\gamma$ , for the first and second modes. The train loads position on the beams are defined according to their group velocity,  $v$ , and their starting positions at  $t = 0$  is  $x = s_p L$

$$\xi_p = \frac{s_p L + vt}{L} = s_p + \frac{v}{\omega_1 L} \tau \quad (19)$$

The non-dimensional location of the  $p$ th moving load,  $\xi_p$ , is used in time-varying train mass matrix,  $M_{ij}^t$ , and train load vector,  $F_j^{t*}$  by the term  $\pi \xi_p$  (see equation (13)). This term is redefined as  $\Omega_l \tau + \theta$  where,

$$\Omega_l = \frac{\pi v}{\omega_1 L} \quad (20)$$

and,  $\theta = \pi s_p$ . The non-dimensional speed of the lateral motion,  $\Omega_l$ , is an important parameter of the system.

Alexander and Kashani (2018) investigated bridge deck-train interaction considering vertical motion of the deck and found that the non-dimensional speed of the vertical motion plays a key role in dynamic behaviour of the deck. For the non-dimensional speed of the vertical motion,  $\Omega_v$ , the frequency of the first flexural mode of the deck was used. For the non-dimensional speed of the lateral motion, however, the frequency of the first lateral flexural mode of the pier-deck system is used. At the supports, the two parallel tubes are likely to act compositely as they will be connected by a supporting beam. We consider the case where, for the majority of the tubes' length away from the supports, the tubes have no connecting beams. So, there is no shear transfer between tubes and they act as independent parallel beams. Hence, the flexural rigidity around both horizontal and vertical axes of the deck is assumed identical in this study. Employing the mean frequency suggested in (Network Rail,

2006), Alexander and Kashani (2018) related the non-dimensional speed of vertical motion to the span length for a wide range of train speeds. They recommended that the mean HS train reaches a vertical non-dimensional speed range of 0-1/3 independent of span length, and Hyperloop/Transpod trains experience a vertical non-dimensional speed range of 0-4/3. For the lateral vibration, non-dimensional speed limits are determined for HS trains and Hyperloop/TransPod trains:

$$\Omega = \pi^2 \sigma \Omega_v, \quad \Omega_v = \frac{\pi v}{\omega_{1v} L}, \quad (21)$$

in which  $\omega_{1v}$  is the first natural frequency of the unload bridge for vertical motion. Thus, by parametrically varying  $\Omega$  we explore the influence of both train speed and span length.

### 3. Lateral Dynamic Amplification Factor

To study the effects of moving train on lateral motion of pier-deck system, lateral dynamic amplification factor (DAF),  $\lambda$ , is determined and compared for a wide range of key parameters:

$$\lambda = \frac{y_d^{\max}(\tau, \xi)}{y_s^{\max}(\tau, \xi)} \quad (22)$$

where  $y_d^{\max}$  and  $y_s^{\max}$  are absolute maximum dynamic and quasi-static lateral deflections.

Note that the location of both the maximum quasi-static and dynamic deflection is dependent on geometry and speed. For example, in the dynamic case, the maximum deflection occurs near to the modal maximum of the predominant mode for a given speed. This location will not generally be a midspan. For very low pier-to-deck stiffness ratios, the maximum deflection could be at a pier, while for high pier-to-deck stiffness ratios, it is likely to be nearer to a midspan. Eq. (22) simply determines the maxima DAF regardless of the specific locations of the maxima of quasi-static and dynamic deflections.

The dynamic deflection is determined from solving equation (12), and the quasi-static deflection is obtained setting inertial and damping terms of equation (12) equal to zero. The

parameters of bridge deck-pier systems are: (1) lateral non-dimensional speed,  $\Omega_l$ , (2) number of moving masses for train,  $n_p$ , (3) number of spans of length  $L$ ,  $n_s$ , (4) single train-to-single span bridge mass ratio,  $\alpha_p$ , (5) the spacing between moving loads,  $s_p$ , (6) pier-to-deck stiffness ratio,  $\eta_k$ , (7) eccentricity ratio,  $e$ , and (8) damping ratio of the first and second modes of the beams,  $\gamma$ , where identical damping ratio is assumed for both modes. Note that any variation in train loading eccentricity does not change the lateral DAF. This is because the train loading (see equation (10)) and accordingly lateral deflection of the system (equation (12)) is linearly related to the eccentricity ratio,  $e$ .

Figure 2 shows an example of the first three mode shapes and modal frequencies ( $f_1, f_2$ , and  $f_3$ ) for a 4-span bridge with flexible and stiff columns, and  $\Omega_l = 1$ . As expected, for the bridge with flexible columns, the mode shapes have nonzero values at the supports (see Figure 2a) while the modal coords are very close to zero at the supports for the bridge with stiff columns (see Figure 2b). Further, the bridge with stiffer columns has higher modal frequencies as expected.

Figure 3a shows the solution of equation of motion (equation (13)) for both dynamic and quasi-static states at the midspan location of a single-span bridge with  $\Omega_l = 0.3$ ,  $\alpha_p = 0.1$ ,  $\eta = 100$ ,  $e = 0.1$ , and  $\gamma = 0.05$ . The horizontal axis is normalised by  $\pi / \Omega_l$  which is the non-dimensional traverse time of the moving mass across the span length  $L$ . Hence, at  $\pi / \Omega_l = 1$ , the moving mass has travelled the single-span bridge, and for  $\pi / \Omega_l$  values higher than 1, the moving load is not on the bridge, and the bridge freely vibrates. The temporal variation of dynamic and quasi-static deflections are not identical and the position and magnitude of maximum dynamic and quasi-static deflections are also different. Figure 3b displays the temporal variation of the lateral dynamic-to-static deflection ratio ( $y_d/y_s$ , dashed-to-solid line

ratio). It is apparent that the maximum lateral deflection ratio does not occur when the load is exactly at the midspan but very close to the midspan.

### 3.1 Effect of number of spans and train-to-bridge mass ratio

Figure 4 shows the effects of number of spans on the DAFs for the lateral vibration. Lateral DAFs are plotted versus non-dimensional speed for single-span to 5-span beams. This figure is for case of single moving mass ( $p = 1$ ) on a continuous beam. The results demonstrate a maximum which increases for higher number of spans. The increase in the peak is because of the train loading being in contact with the beam for more cycles of loading. Hence, the higher the number of span is, the more dominate the resonant response is. The maximum speed limits for HS trains and Hyperloop trains form regions as the natural frequency of the unload bridge changes for different number of spans. It is favoured that the current maximum speed for HS trains falls below this resonance, and that the continuous spans do not extend to high  $n_s$  practically without using thermal expansion joints. It is worth noting that the worldwide average speed of conventional HS trains is around 270 km/h ( $0 < \Omega_l < 1/3$ ) which suggests  $\lambda \leq 1.55$ . It should be noted that unequal spans might affect the results and need further research. It is a function of flexural rigidity of the deck and pier as well as the ratio of each span length to the total length of the bridge.

Figure 5 shows lateral DAFs of a 4-span beam with different train-to-bridge mass ratios (mass ratios,  $\alpha_p = 0.1, 0.3, 0.5$ , and  $1.0$ ). The maximum speed limits for HS trains and Hyperloop trains are constant as the natural frequency of the unload bridge remains unchanged for different mass ratios. It is worth noting that as the mass ratio increases, the lateral DAF does so. Furthermore, the maximum lateral DAF moves toward lower non-dimensional speed with the increase of mass ratio. Comparison of the DAF range in (Alexander & Kashani 2018) with those determined in the current study, suggests that DAF of vertical vibration are much larger than those from lateral vibration.

### 3.2 Effect of spacing of train masses

Figure 6 illustrates lateral DAFs versus non-dimensional speed and spacing for a train of 9 equidistance masses. In the case where  $s_p$  is zero, a single moving mass travels the bridge while for non-zero  $s_p$  values, the mass of each moving load is  $0.2/9$ . Thus, the total mass ratio between the train and the deck is assumed to be 0.2. The maximum lateral DAFs are roughly similar to a single moving mass case ( $s_p = 0$ ). However, the maximum lateral DAFs for spacing range of 0.1-0.15 is slightly lower than those for other spacing ratios. Further, the speed at which the maximum lateral DAF occurs depends on the spacing ratio. As spacing ratio increases, the maximum lateral DAF moves towards higher non-dimensional speeds. For normal HS trains, this is very desirable as it pushes the resonance further away from their operating speed limit. However, for Hyperloop trains, it is adverse as this effect pushes the resonance close to their operating speed limit.

### 3.3 Effect of pier-to-deck stiffness ratio

Figure 7 shows lateral DAFs versus non-dimensional speed and column-to-beam stiffness ratio, i.e. lateral flexural rigidity of the column to that of the deck. Like the effect of spacing of train masses (see section 3.2), the maximum lateral DAFs at the resonance are quite similar. The speed corresponding to the maximum lateral DAFs also depends on the stiffness ratio. This speed increases for higher stiffness ratios which is very beneficial for conventional HS trains. However, it is critical for Hyperloop trains when the stiffness ratio is very large and the resonant speed becomes closer to operating speed limit Hyperloop trains.

When the pier is very flexible particularly in post-tensioned spinal rocking piers ((Kashani et al. 2018),(Kashani et al. 2019), (Ahmadi & Kahshani 2019)), the lateral vibration of the bridge deck becomes very large and lateral vibrations could be critical even for small lateral DAFs from design point of view. However, large lateral flexibility is desirable for earthquake resistant design of a bridge as high lateral displacements cause high energy dissipations.



#### 4. Conclusions

Dynamic amplification factors of Hyperloop trains for lateral vibration were addressed through a parametric analysis. The Hyperloop train-bridge-pier system were analytically modelled and described in form of a series of non-dimensional parameters.

It was found that lateral DAFs of the system are highly dependent on the train speed, train-to-bridge mass ratio, train loading spacing, and pier-to-deck stiffness ratio. At a specific train velocity, a peak is seen in DAFs of the system. Higher number of spans and train-to-bridge mass ratios respectively increase and decrease the peak DAF. The effect of spacing of train loading and pier-to-deck stiffness ratio on maximum DAFs are negligible.

Note also that the maximum lateral DAFs (a maximum of approximately 2, for 5% damping) are much lower than those observed for vertical motions (a maximum of 10, for 5% damping) in [2]. Nevertheless, in both cases these are significantly larger than code recommendations.

While the DAFs of lateral vibration are much smaller than the vertical vibration, it does not lower the importance of lateral vibrations as small lateral vibrations of the bridge deck can cause or enhance the bridge pier uplift. Slight lateral vibrations can also have negative impacts on the train stability or cause passengers discomfort at high speeds. Therefore, this work highlights the significance of lateral vibration in addition to the vertical vibration for Hyperloop train-bridge-pier systems which needs be considered in future design guidelines.

The current study investigates dynamic amplification factors under one moving trainset with constant velocity. This means further works on multi moving trainsets crossing each other even for accelerating and decelerating cases are required. Furthermore, the present work focuses on straight train track, and further work on curved bridges is required due to potentially high effect of centrifugal forces on lateral vibration of the deck. Rigorous nonlinear finite element analyses are also needed to better understand the dynamics of the Hyperloop train-bridge-pier systems.

## Acknowledgement

The first author acknowledges support received by the UK Engineering and Physical Sciences Research Council (EPSRC) for a Prosperous Nation [grant number EP/R039178/1: *SPINE: Resilience-Based Design of Biologically Inspired Columns for Next-Generation Accelerated Bridge Construction*].

## Notation

$m_p$	is the mass of the $p$ th load
$\beta(x)$	boxcar function
$H(x)$	is the Heaviside function
$V$	the potential energy
$\Pi$	is the Lagrangian
$u_j$	is the lateral displacement at the $j$ th support
$M_{ij}^b$	is the bridge mass matrix
$M_{ij}^t$	is the travel load (trainset) mass matrix
$K_{ij}^b$	is the bridge (deck beam) stiffness matrix
$K_{ij}^c$	is the supports (columns) stiffness matrix
$\omega$	is the frequency parameter
$\varepsilon$	is an eccentricity ratio
$\tau$ and $z$	are normalised time and displacement respectively
$\gamma$	damping ratio
$v$	group velocity

## References

- Ahmadi, E. & Kashani, M.M., 2019. On the use of entangled wire materials in pre-tensioned rocking columns. *Journal of Physics: Conference Series*, 1264(2019) 012006, doi:10.1088/1742-6596/1264/1/012006.
- Alexander, N.A. & Kashani, M.M., 2018. Exploring Bridge Dynamics for Ultra-high-speed, Hyperloop, Trains. *Structures*, 14(February), 69–74.  
<https://doi.org/10.1016/j.istruc.2018.02.006>.
- Anon, 2003. British Standard, EN 1991-2: Eurocode 1: Actions on structures in: Part 2: Traffic loads on bridges. *European Committee for Standardization*.
- Anon, 2006. Network Rail, NR/GN/CIV/025 Issue 3, Guidance note – the structural assessment of underbridges.
- Canning, L. & Kashani, M.M., 2016. Assessment of U-type wrought iron railway bridges. *Proceedings of the ICE - Engineering History and Heritage*, 169(2).
- Caprani, C.C. & Ahmadi, E., 2016. Formulation of human-structure system models for vertical vibration. *Journal of Sound and Vibration*. 377, 346–367.  
<https://doi.org/10.1016/j.jsv.2016.05.015>.
- Cruz, C. & Miranda, E., 2017. Evaluation of the Rayleigh damping model for buildings. *Engineering Structures*, 138, 324–336.  
<http://dx.doi.org/10.1016/j.engstruct.2017.02.001>.
- E., M., *Hyperloop alpha. hyperloop alpha design proposal, SpaceX (Online Article)*. URL. [http://www.spacex.com/sites/spacex/files/hyperloop\\_alpha.pdf](http://www.spacex.com/sites/spacex/files/hyperloop_alpha.pdf),
- Filho, F. V., 1978. Finite Element Analysis of Structures Under Moving Loads. *The Shock and Vibration Digest*, 10, 27–35.
- Fřýba, L., 1972. *Vibration of solids and structures under moving loads*,
- Janzen, R., 2017. TransPod Ultra-High-Speed Tube Transportation: Dynamics of Vehicles and Infrastructure. *Procedia Engineering*. 8–17.

- Kashani, M.M. et al., 2018. Experimental investigation of a novel class of self-centring spinal rocking column. *Journal of Sound and Vibration*, 437, 308–324.  
<https://doi.org/10.1016/j.jsv.2018.08.034>.
- Kashani, M.M. et al., 2019. Layered composite entangled wire materials blocks as pre-tensioned vertebral rocking columns. *Composite Structures*, 214, 153–163.  
<https://linkinghub.elsevier.com/retrieve/pii/S0263822318332690>.
- Olsson, M., 1985. Finite element, modal co-ordinate analysis of structures subjected to moving loads. *Journal of Sound and Vibration*, 99, 1–12.
- Olsson, M., 1991. On the fundamental moving load problem. *Journal of Sound and Vibration*, 145, 299–307.
- Parke, G. & Hewson, N., ICE manual of bridge engineering. 2nd edition Thomas Telford publishing.
- Paultre, P., Chaallal, O. & Proulx, J., 1992. Bridge dynamics and dynamic amplification factors — a review of analytical and experimental findings. *Canadian Journal of Civil Engineering*, 19(2), 260–278.
- Timoshenko, S.P., 1922. On the forced vibrations of bridges. *The London, Edinburgh, and Dublin Philosophical Magazine and Journal of Science*, 46, 1018–1019.
- Wu, J., Whittaker, A. & Cartmell, M., 2000. The use of finite element techniques for calculating the dynamic response of structures to moving loads. *Computers & Structures*, 78, 789–799.

**Figure captions**

Figure 1. A train composed of a set of  $p$  moving point masses traveling across two continuous  $n_s$ -span Hyperloop tube beams supported by  $n_s+1$  columns.

Figure 2. The first three mode shapes of a 4-span bridge and their frequencies: (a)  $\eta = 100$ , and (b)  $\eta = 10000$ .

Figure 3. (a) Midspan ( $\xi = 0.5$ ) lateral deflection of the beams (quasi-static versus dynamic), and (b) lateral dynamic-to-static deflection ratio versus scaled time.

Figure 4. Lateral dynamic amplification factors for various number of spans,  $n_s$ ,  $\alpha_p = 0.1$ ,  $\eta = 100$ ,  $e = 0.1$ , and  $\gamma = 0.05$ .

Figure 5. Lateral dynamic amplification factors for various mass ratios,  $\alpha_p$ ,  $n_s = 4$ ,  $\eta = 100$ ,  $e = 0.1$ , and  $\gamma = 0.05$ .

Figure 6. Lateral dynamic amplification factors for various moving mass spacing ratios,  $\alpha_p = 0.2/9$ ,  $\eta = 100$ ,  $n_s = 4$ ,  $e = 0.1$ , and  $\gamma = 0.05$ : (a) 3D plot, and (b) contour plot.

Figure 7. Lateral dynamic amplification factors for various column-to-beam stiffness ratios,  $\alpha_p = 0.2$ ,  $n_s = 4$ ,  $e = 0.1$ , and  $\gamma = 0.05$ : (a) 3D plot, and (b) contour plot.

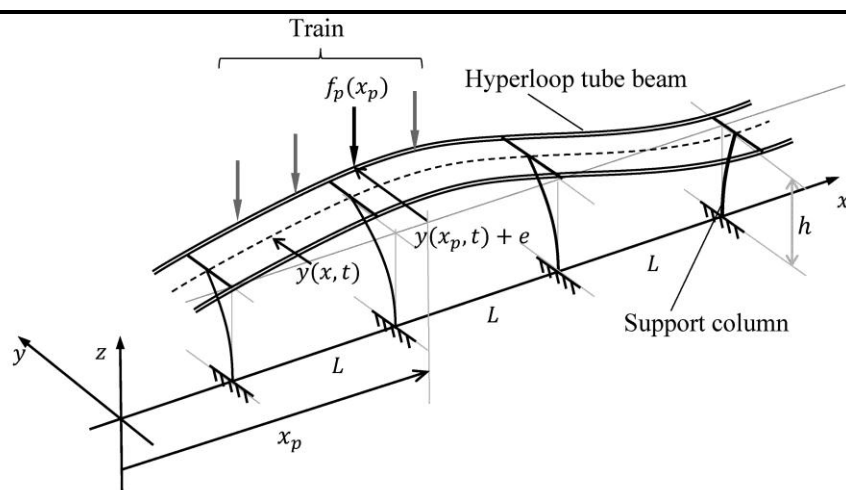


Figure 1

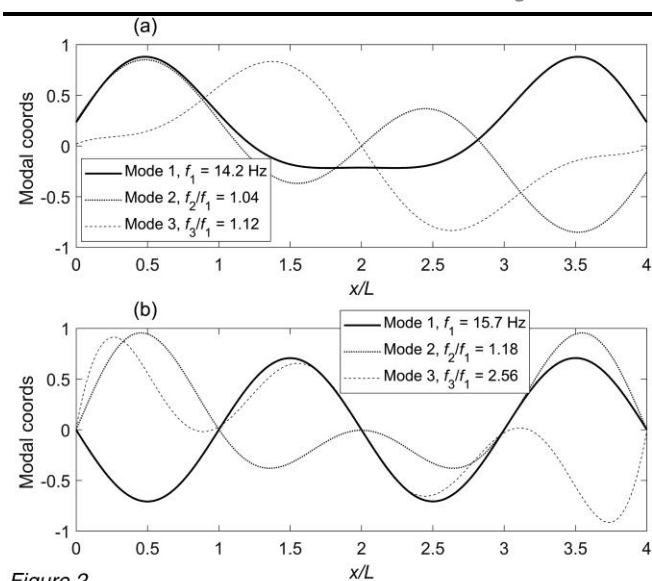


Figure 2

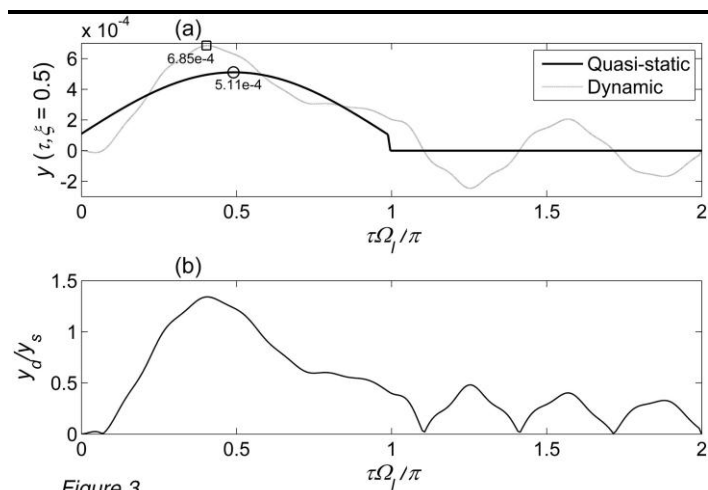


Figure 3



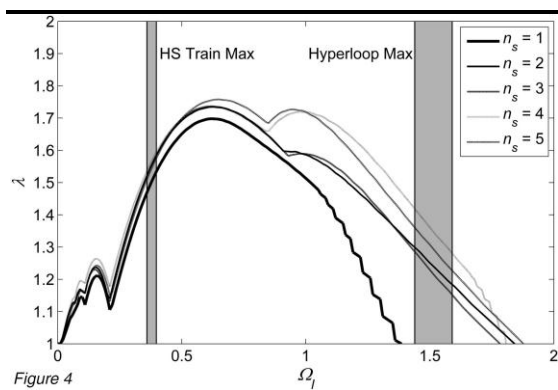


Figure 4

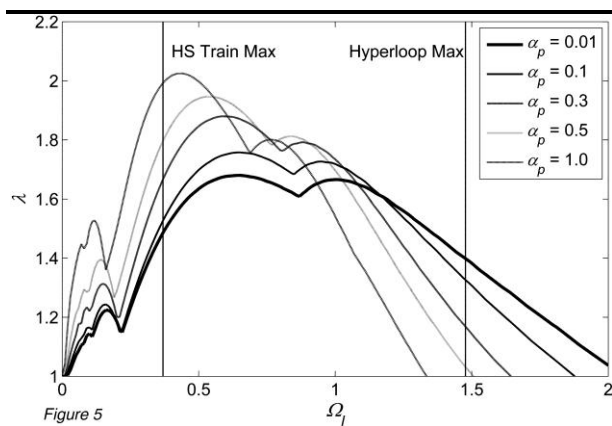


Figure 5

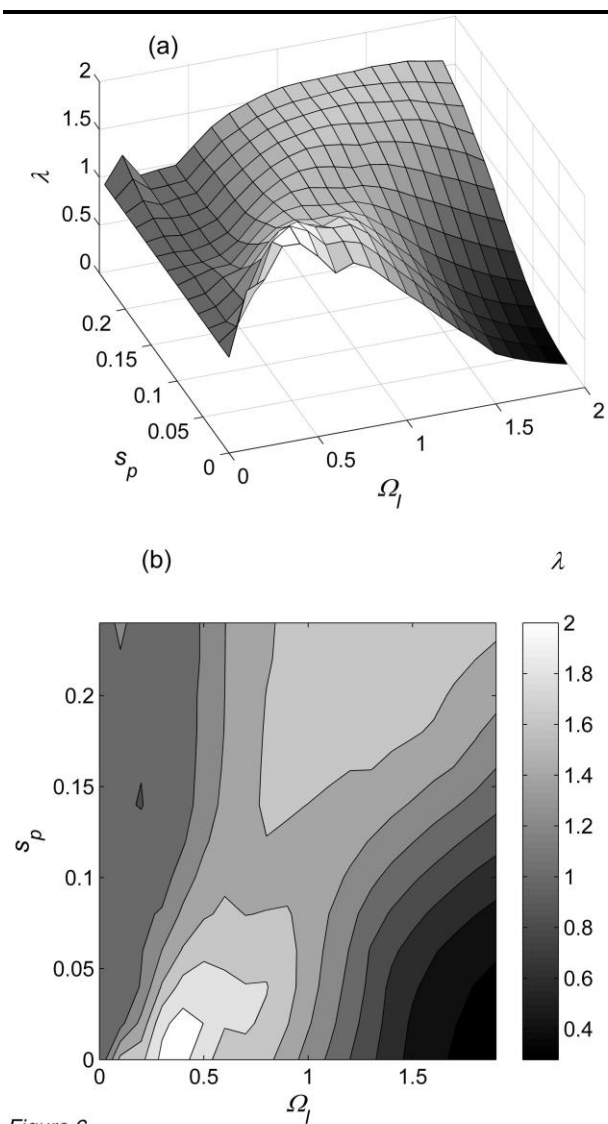


Figure 6

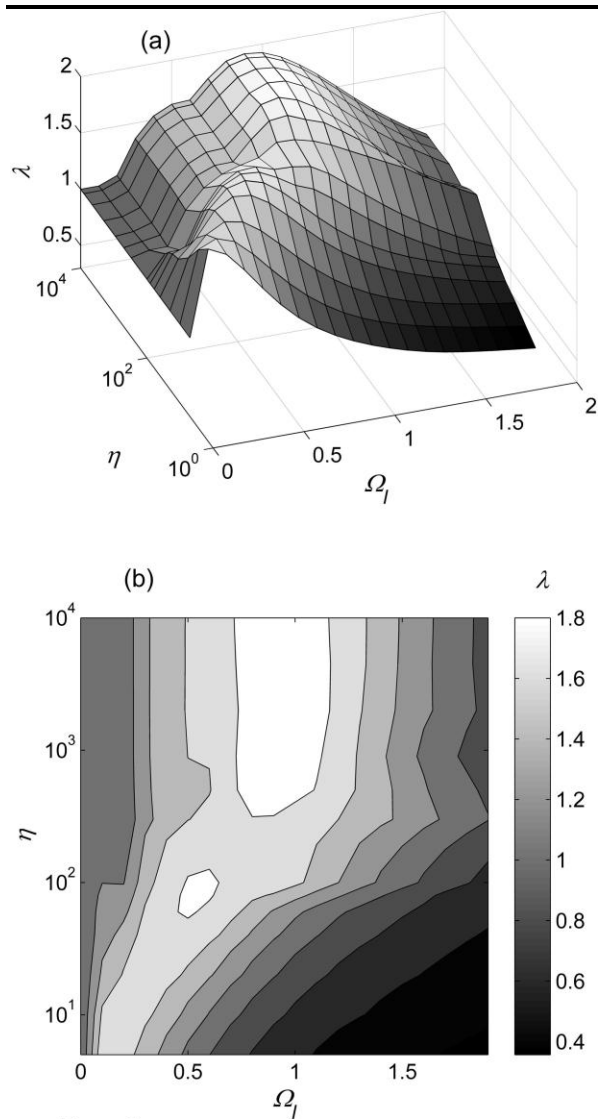


Figure 7